



## Article

# Research on Precise Tracking Control of Gear-Shifting Actuator for Non-Synchronizer Automatic Mechanical Transmission Based on Sleeve Trajectory Planning

Xiangyu Gongye <sup>1</sup>, Changqing Du <sup>1,\*</sup> , Longjian Li <sup>1</sup>, Cheng Huang <sup>1</sup>, Jinhai Wang <sup>1</sup>  and Zhengli Dai <sup>2</sup>

<sup>1</sup> Hubei Key Laboratory of Advanced Technology for Automotive Components, Wuhan University of Technology, Wuhan 430070, China; gongyexiangyu1992@whut.edu.cn (X.G.); li\_longjian@whut.edu.cn (L.L.); 196459@whut.edu.cn (C.H.); wangjinhai@whut.edu.cn (J.W.)

<sup>2</sup> Chongqing Tiema Industries Group Co., Ltd., Chongqing 400050, China; ctm@tiemagroup.com

\* Correspondence: cq\_du@whut.edu.cn

**Abstract:** The Non-Synchronizer Automated Mechanical Transmission (NSAMT) demonstrates a straightforward structure and cost-effectiveness; however, the primary obstacle to its widespread application lies in NSAMT shift control. The implementation of active angle alignment effectively addresses the issue of shifting quality, but achieving active angle alignment necessitates precise tracking of the planned shifting curve by the gear-shifting actuator. To tackle the control problem of accurate tracking for NSAMT shift actuators, this paper initially analyzes the structure and shift characteristics of the NSAMT. Based on this analysis, a physical model is established using Amesim, incorporating a drive motor, two-gear NSAMT, shift actuator, sleeve, and DC motor model. An extended state observer (ESO) is designed to mitigate unknown interference within the system. Furthermore, an active angle alignment control algorithm based on “zero speed difference” and “zero angle difference” for double target tracking is constructed while planning the axial motion trajectory of the sleeve. The Backstepping algorithm is employed to successfully track and regulate this planned trajectory. Finally, through Hardware-in-the-Loop testing, we validate our proposed control strategy, which demonstrates consistent results with simulation outcomes, thereby affirming its effectiveness.

**Keywords:** Non-Synchronizer Automated Mechanical Transmission; active angle alignment; shift actuator control; algorithm design



**Citation:** Gongye, X.; Du, C.; Li, L.; Huang, C.; Wang, J.; Dai, Z. Research on Precise Tracking Control of Gear-Shifting Actuator for Non-Synchronizer Automatic Mechanical Transmission Based on Sleeve Trajectory Planning. *Energies* **2024**, *17*, 1092. <https://doi.org/10.3390/en17051092>

Academic Editor: Atriya Biswas

Received: 15 January 2024

Revised: 17 February 2024

Accepted: 20 February 2024

Published: 25 February 2024



**Copyright:** © 2024 by the authors. Licensee MDPI, Basel, Switzerland. This article is an open access article distributed under the terms and conditions of the Creative Commons Attribution (CC BY) license (<https://creativecommons.org/licenses/by/4.0/>).

## 1. Introduction

The NSAMT exhibits the advantages of cost-effectiveness, high transmission efficiency, and low development expenditure, rendering it a pivotal avenue for advancing electric vehicle transmission systems [1–5]. Nevertheless, the AMT suffers from power interruption during gear changes and significant shift impact, which constitute its primary drawback [6,7]. The synchro-less automatic mechanical transmission structure, depicted in Figure 1, showcases a simplified design and cost-effectiveness by seamlessly integrating the motor with the AMT while eliminating components such as the clutch, synchronization ring, and friction cone.

In the examination of the AMT shift process, scholars have generally categorized it into six stages [1,8,9] and provided detailed descriptions and analyses for each stage. The conventional AMT shift control involves the engagement of the target gear by the shift actuator after the completion speed adjustment (when the difference between sleeve speed and target gear speed reaches a certain threshold). However, this method is susceptible to meshing tooth collision, as depicted in Figure 2a,b.

In the NSAMT shift process, a higher level of efficiency is achieved through the coordinated control of the shift actuator and drive motor. The drive motor exhibits rapid response and precise torque and speed adjustment capabilities [10], enabling active synchronization

between the sleeve speed and target gear speed without relying on the synchronization ring and friction cone. The sleeve effectively engages the target gear for power transmission, minimizing shifting impact and reducing overall shifting time [6]. Despite its simple structure and cost-effectiveness, coordinating the control of the shift actuator and drive motor remains a significant challenge.

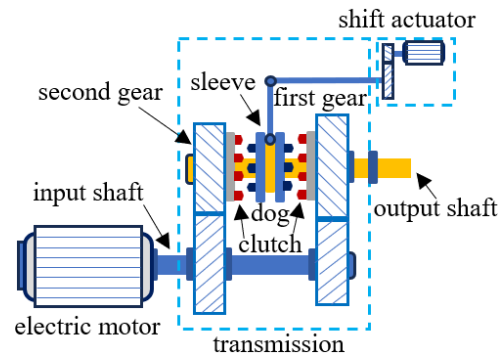


**Figure 1.** The structure of NSAMT.

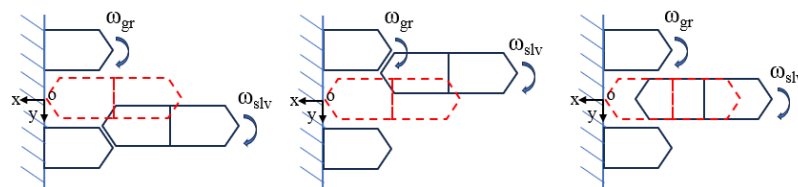


**Figure 2.** Process of bonding sleeve and target gear engagement.

### 1.1. Survey of AMT Shift Control

The paper [11] presents the design of an extended state observer (ESO) by Shuai Wang et al., which effectively addresses the issue of unknown interference in the system. By employing the Backstepping method, they derive the final control rate to achieve accurate position tracking of the actuator. Simulation results demonstrate that this controller enables rapid response and high control accuracy, thus validating its efficacy. Y Lei et al. [2] proposed a double closed-loop PID control system based on fuzzy self-adaptation, and simulation results demonstrate that the shift actuator achieves stability within 130 ms, exhibiting fast response speed, high control accuracy, and excellent stability. In [12–15], an electromagnetic actuator is designed, and ADRC is employed to enhance the tracking accuracy of the synchronization process. The comparison between simulation and experimental results validates the effectiveness of the proposed control approach, offering a novel solution for AMT gear-shifting systems. The authors of a study (Tao P et al. [16]) developed a hierarchical pattern optimization strategy (HMOS) for AMT gear junction, wherein GEP models were established for the shift actuator and three stages to reveal the relationship between sleeve displacement and friction cone torque. At the top layer of the HMOS, a novel sliding mode predictive controller (SMPC) with constraints was proposed for making tapered torque decisions during the GEP synchronization phase. The bottom layer of the HMOS introduces an MPC-based trajectory-tracking controller, which is integrated with a load torque disturbance observer (L-DOB). Finally, the proposed control strategy was simulated and tested using HIL, successfully verifying its optimized performance in terms of longitudinal shift impact, synchronizer slip work, and thermal stress. The paper [17] proposes an optimal discrete-time control scheme for an AMT motor-driven shift actuator, which consists of state feedback, discrete integrator, and preview control. Preview feedforward control utilizes future reference signal information to proactively regulate the shift actuator, ensuring excellent position-tracking performance even in the presence of torque disturbances. Both simulation and test bench results demonstrate that the proposed

preview control algorithm can achieve rapid and accurate position-tracking control without significant overshoot or steady-state errors while maintaining high-quality gear shifting. The shift control effect of an automated manual transmission (AMT) and reduction in synchronizer wear were optimized by implementing a variable parameter control method based on current feedback during the transmission bench test, as discussed in [18]. Shift tests were conducted in groups to investigate the influence of shift stroke and speed on the duration of each stage's shifting process. The maximum force required for shifting by the synchronizer was calculated and analyzed based on the results obtained from each group. Experimental findings demonstrate that the utilization of current feedback in the variable parameter control method effectively optimizes the relationship between shift time and synchronizer wear. The paper [5] proposes a control strategy for coordinating the speed of the drive motor and the displacement of the shift motor in an integrated motor transmission (IMT) system during shifting. To achieve active speed synchronization in the IMT system, a polynomial speed trajectory is utilized to redesign the reference speed of the drive motor. In order to ensure fast and reliable tracking of sleeve position under load disturbances during shifting, a robust optimal preview controller is developed for the shift motor. Coordinated control is performed based on signals from both drive motor speed and sleeve axial position. A joint simulation using Matlab/Simulink and Amesim is conducted to demonstrate the dynamic characteristics of the IMT system throughout the entire shifting process, while a comparative simulation test showcases the effectiveness and performance of this proposed control strategy.

During the shifting process, a significant disparity in speed between the engaging sleeve and the gear ring to be engaged can result in prolonged shifting duration, substantial impact during shifting, and even failure to complete the shift. Recent research has extensively explored active angle alignment control as a means of synchronizing the speed of the sleeve with that of the target gear through coordinated regulation of the shift actuator and drive motor [19–21]. This approach aims to minimize shift time and mitigate impact during shifting [6,14,22]. As a result of the precise control of the engagement of the sleeve with the target gear, the teeth of the sleeve can smoothly enter the tooth groove of the gear ring without any collision, thereby achieving a shifting process characterized by minimal impact and zero tooth collision. By actively regulating the torque of the drive motor, Tian Feng et al. [19] successfully achieved dual-target-tracking control, ensuring “zero speed difference” and “zero angle difference” between the relative speed and relative angle of the sleeve and coupling gear ring. To mitigate tooth impact resulting from frequent switching between drive and brake quadrants during active synchronous control of the drive motor, an optimal torque active angle alignment algorithm was proposed to minimize quadrant switching times. Using the principle of multi-body dynamics, Zeng Yuanfan [20] developed a hybrid automaton model that accurately depicts the dynamic characteristics of the gear-shifting process. Based on each stage's dynamic characteristics in the model, a gear-shifting control strategy incorporating speed active synchronization and angle active synchronization is devised to ensure precise synchronization between the sleeve and joint gear ring during gear shifts. The collision process between the sleeve and the target gear ring, considering tooth-side chamfering, was analyzed and simulated by Xiaotong Xu et al. [14,21]. The collision stiffness was calculated using the Monte Carlo method and equivalent depth. Based on this, a coordinated shift control method is proposed for the NSAMT. In this method, speed synchronization is performed when the speed difference between the engaging sleeve and the target meshing gear reaches a certain threshold value. Subsequently, angle synchronization is utilized to quickly align the engaging sleeve with the predicted target gear groove obtained from an active angle alignment algorithm. Simulation and bench test results demonstrate that this control method can effectively reduce shift duration and minimize maximum impact. The dynamic model of the shifting process was initially derived as a hybrid automaton (HA) model by Ziwan Lu et al. [6,22]. Subsequently, utilizing the minimum principle of Pontryagin, they solved for the time-optimal control law of synchronous speed and angle to achieve zero speed

and angle difference, thereby reducing shifting time. Additionally, in order to address the issue arising from periodic changes in rotation angle difference, an optimal initial angle difference was introduced, followed by its replacement with incremental angle difference. Building upon this foundation, a model tracking strategy is proposed to enhance a system's anti-jamming capability.

### 1.2. Problem Description

Active angle alignment control prevents the occurrence of gear ring collision during gear shifting and effectively mitigates the impact experienced during this process. This control mechanism fulfills the NSAMT's requirement for swift and seamless movement of the sleeve from the neutral position to the desired gear position in gear shifting, making it highly applicable for process control in hybrid electric vehicles or pure electric vehicles equipped with the NSAMT. In the process of active angle alignment, two crucial issues are the planning of the axial motion trajectory of the sleeve and the track tracking of the gear-shifting actuator. Among them, prior to track tracking, motion trajectory planning for the gear-shifting actuator is an independent task. Most existing research on active angle alignment algorithms adopts a control method that first achieves speed synchronization and then angle synchronization. While this method enables collision-free coupling between the sleeve and target gear ring, it unavoidably prolongs tooth meshing time due to sequential speed and angle synchronization. Moreover, there is a possibility that the sleeve may exceed its original target tooth position, requiring re-alignment of teeth which not only extends tooth meshing time but also reduces success rate. The axial motion trajectory of the sleeve is meticulously planned and synchronized with the rotation angle, ensuring that speed regulation commences only after gear retreat is completed and simultaneous movement of the sleeve occurs. During speed synchronization, the teeth of the sleeve smoothly engage into the tooth groove of the target gear ring without any collision, as illustrated in Figure 3. This method of synchronously adjusting rotational speed and rotation angle not only governs the circumferential motion of the sleeve but also necessitates careful planning of its axial motion trajectory. However, this active angle alignment method for planning sleeve trajectories has been scarcely reported both domestically and internationally; nevertheless, it can be theoretically realized based on existing control methods.

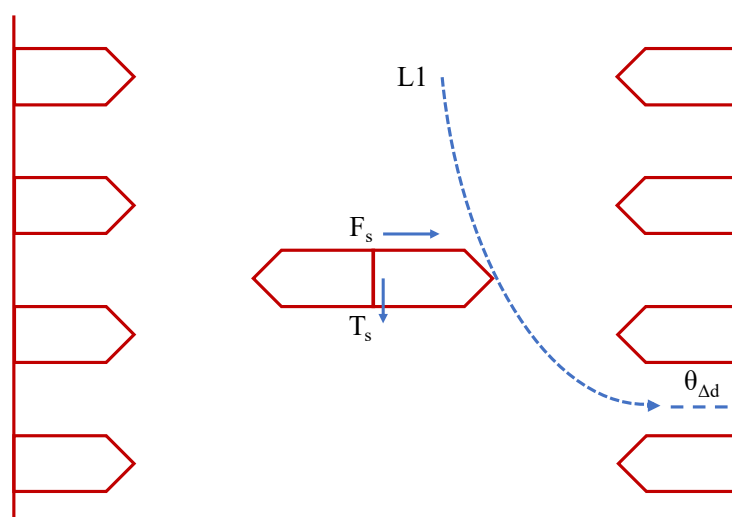


**Figure 3.** Schematic diagram of active angle alignment process.

In addition, accurate and real-time tracking and controlling of the gear-shifting actuator's trajectory based on the motion trajectory of the sleeve is a crucial aspect of active angle alignment control. The process of trajectory tracking involves nonlinearities and uncertain interferences. Furthermore, considering the precision of component manufacturing and

wear during operation, it is essential to account for uncertain changing parameters that cannot be ignored, thereby making the control problem more challenging. Amongst numerous studies on track-tracking control for AMT gear-shifting actuators, some focus solely on controlling fixed values for gear-shifting actuators, however, their methods are unsuitable for tracking nonlinear trajectories. In the study of nonlinear trajectory tracking, various control algorithms have been employed by different researchers, including Backstepping, LQR, active disturbance rejection control, sliding mode control, model predictive control, and others. Furthermore, the structure of the NSAMT differs from that of the traditional AMT in that the NSAMT does not require speed synchronization through friction cones and synchronization rings during shifting processes; as a result, the system states are distinct from those observed in the traditional AMT. A comparison between these two structures is presented in Figure 4.

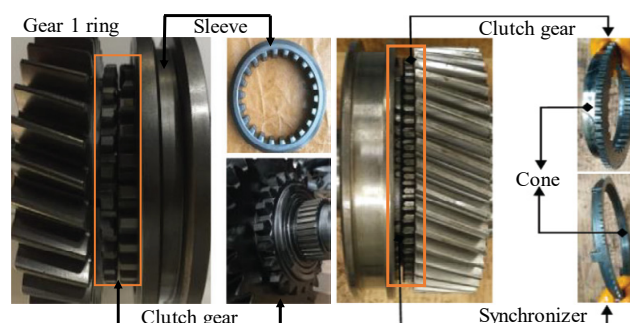


**Figure 4.** Comparison between NSAMT structure and traditional AMT structure.

### 1.3. Motivations and Innovations

According to the aforementioned analysis, achieving active angle alignment control and minimizing meshing tooth collision during gear shifting hinges on meticulously planning the movement trajectory of the sleeve. It also necessitates addressing nonlinear and uncertain interference issues in the track-tracking process of the gear-shifting actuator, as well as designing a real-time and accurate track-following control system. Therefore, it is imperative to investigate an active angle alignment control method based on trajectory planning of the gear sleeve for enhancing the NSAMT's gear-shifting quality. This entails ensuring precise motion trajectory tracking by the gear-shifting actuator to reduce active angle alignment time effectively while eliminating any potential collisions between gears during engagement.

The contributions or innovations of this paper are summarized as follows:

- (1) According to the unique structure of the NSAMT, a comprehensive analysis is conducted on the dynamic characteristics of the NSAMT during the shifting process, with a particular emphasis on the time-varying resistance characteristics in the “gear against” stage.
- (2) This paper proposes an active angle alignment method based on axial trajectory planning of the sleeve, which serves as a reference for controlling tooth insert gears with improved precision and efficiency.
- (3) By designing a Backstepping method based on the axial trajectory planning of the engaging sleeve, accurate tracking and control of its axial trajectory can be achieved by the shifting actuator. This facilitates collision-free engagement between the engaging sleeve and the target engaging gear ring.

### 1.4. Outline

The remaining sections of this article are structured as follows: The second section examines the gear-shifting actuator and establishes the Amesim (2020) model. In the third section, an axial motion trajectory for the sleeve is planned based on active angle alignment, followed by the design of precise tracking control for the NSAMT shift actuator using

sleeve trajectory planning. The fourth section presents a joint simulation analysis of the proposed control strategy using Matlab/Ameism (MATLAB R2020b). Finally, HIL testing verifies the last part and draws conclusions.

## 2. System Modeling

The dynamic modeling of the controlled object is a prerequisite for analyzing and controlling it. During the shifting process, the NSAMT involves the respective dynamic response and interaction among the sleeve, original gear ring, and target gear ring in the transmission system. Therefore, prior to studying the NSAMT shift control algorithm, it is essential to first establish a model of the NSAMT shift system and its shifting process.

### 2.1. Shift Process Analysis

The key components of the NSAMT system, including the spline hub, sleeve, and engaging gear rings at each gear position, are illustrated in Figure 4. In this transmission system, the shifting process involves three main sub-processes: lifting gear, synchronizing, and hanging gear. Compared to traditional synchronizer systems with synchronous rings, the NSAMT relies primarily on precise control of the drive motor for synchronization. Additionally, for electric vehicle transmission systems like the NSAMT, the complete shift process consists of five sub-processes: torque reduction before removing the gear; shift removal; synchronization; gear hanging; and torque recovery after completing the gear. Torque reduction occurs when the system is in a specific gear position (e.g., original gear position), while synchronization takes place when it is in a neutral state, and torque recovery happens when it reaches the target gear position. Picking and hanging gears involve crucial interactions between components in both circumferential and axial directions within the NSAMT's sleeve and target coupling gear ring for each respective gear. During the process of removing gears, as motor torque has been unloaded by then, the separation between the sleeve and original gear ring occurs smoothly without further discussion here. This paper solely focuses on analyzing the process from the neutral state to the completion of hanging gears.

In order to achieve a collision-free engagement of the engaging sleeve into the tooth groove of the target gear ring, the sleeve initiates movement from its neutral position until it successfully engages with the target engaging gear ring. During this process, the sleeve is solely subjected to axial shifting force  $F_s$  transmitted by the shifting motor and sliding friction force  $f_s$  between the moving parts and spline hub, as well as circumferential vehicle resistance moment  $T_{load}$ . The kinetic equation of this process can be described as

$$\begin{cases} m_{slv}\ddot{x}_{slv} = F_s - f_s \\ J_{out}\ddot{\theta}_{slv} = -T_{load} \\ J_{in}\ddot{\theta}_{gr} = i_{g0} \cdot i_{g1} \cdot (T_m - T_{fg}) \\ \dot{\theta}_{slv} = \omega_{slv} \\ \dot{\theta}_{gr} = \omega_{gr} \end{cases} \quad (1)$$

where  $m_{slv}$  represents the sleeve's mass;  $\ddot{x}_{slv}$  denotes the axial acceleration of the sleeve;  $\ddot{\theta}_{slv}$  signifies the angular acceleration in the circular direction of the sleeve;  $\ddot{\theta}_{gr}$  indicates the angular acceleration in the circular direction of the joint gear ring;  $\omega_{slv}$  and  $\omega_{gr}$  represent the speeds of the sleeve and coupling gear ring, respectively.  $J_{out}$  is the equivalent moment of inertia at the transmission output end.  $i_{g0}$  is the transmission ratio between the input shaft and intermediate shaft, while  $i_{g1}$  is the transmission ratio between the intermediate shaft and first gear.  $T_m$  stands for motor output torque,  $T_{fg}$  represents mixing resistance within the transmission, and  $J_{in}$  refers to the equivalent moment of inertia at the transmission input end.

The speed and angle discrepancies between the sleeve and the target gear are eliminated during active angle alignment by adjusting the position of the sleeve in terms of

speed and angle. Thus, the differences in speed and angle between the sleeve and the target gear can be expressed as follows:

$$\begin{cases} \Delta\omega_{slv-gr} = |\omega_{slv} - \omega_{gr}| \\ \Delta\theta_{slv-gr} = |\theta_{slv} - \theta_{gr}| \\ \Delta\dot{\omega}_{slv-gr} = \frac{-i_{g0} \cdot i_{g1}}{J_{in}} \cdot T_m + \Delta f \\ \Delta\dot{\theta}_{slv-gr} = \Delta\omega_{slv-gr} \end{cases} \quad (2)$$

The variable  $\omega_{slv}$  represents the speed of the sleeve, while  $\omega_{gr}$  indicates the speed of the target gear.  $\Delta\omega_{slv-gr}$  represents the speed difference between the sleeve and the target gear.  $\theta_{slv}$  represents the angle of the sleeve, and  $\theta_{gr}$  represents the angle of the target gear.  $\Delta\theta_{slv-gr}$  represents the angular difference between the sleeve and the target gear. Additionally,  $\Delta f$  is defined as a constant representing system disturbance.

## 2.2. Shifting Motor and Shifting Actuator Model

The motion trajectory planning of the sleeve necessitates a reliable and precise actuator to achieve rapid and seamless gear meshing. Electromechanical actuators, comprising DC motors and reducers [23], have long been employed in automatic control systems. The DC motor supplies shifting power while the reducer is utilized for torque amplification and speed reduction. Despite variations in parameters among different DC motors and transmission types, their dynamic models can be standardized. Figure 5 illustrates the structure of the NSAMT actuator.

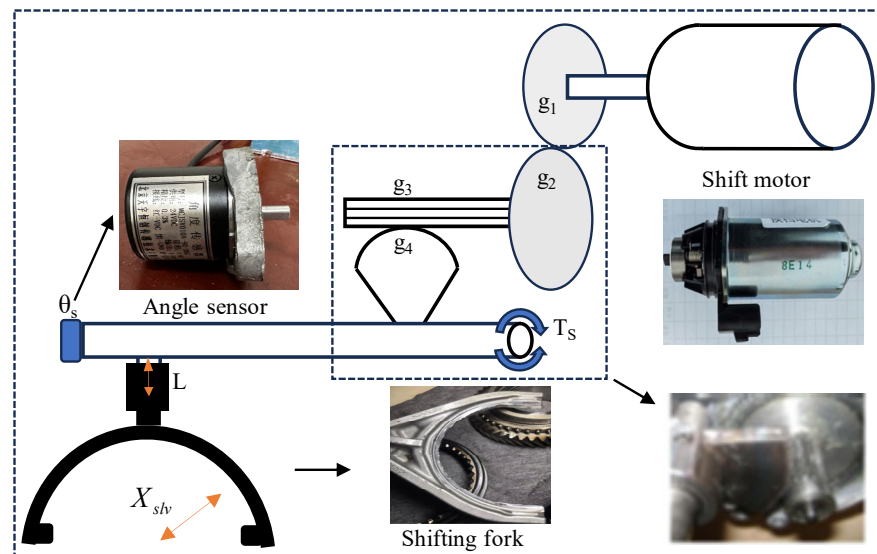


Figure 5. NSAMT actuator structure.

According to Kirchhoff's law and Newton's second law, the dynamics equation of a DC brushed motor is described as follows [24]:

$$\begin{cases} V_{bat} = L_a \frac{di_a}{dt} + R_a i_a + K_e \dot{\theta}_m \\ K_T i_a = J_m \ddot{\theta}_m + b_m \dot{\theta}_m + T_L \end{cases} \quad (3)$$

where  $V_{bat}$  denotes the motor terminal voltage,  $L_a$  denotes the armature inductance,  $i_a$  denotes the armature current,  $R_a$  is the motor resistance,  $K_e$  denotes the counter electromotive force,  $\theta_m$  denotes the motor turning angle,  $K_T$  denotes the torque coefficient,  $T_L$  is the motor load torque,  $J_m$  is the motor moment of inertia, and a further term  $b_m$  is the motor damping coefficient.

There are various types of shift actuators, including ball screws, worm gears, CAM mechanisms, and more. Irrespective of the specific type employed for gear shifting, there exists a definite mathematical relationship between the torque and speed at both ends of the actuator. As depicted in Figure 5, this paper presents a kinematics model of the transmission system for the actuator.

$$\left\{ \begin{array}{l} i_1 = \frac{g_2}{g_1} \\ i_2 = \frac{g_4}{g_3} \\ i_s = i_1 i_2 \\ \theta_m = \theta_s i_s \\ \omega_m = \omega_s i_s \\ x_{slv} = \theta_s L \\ T_s = T_m i_s \\ T_s = F_s L \end{array} \right. \quad (4)$$

where  $g_1$  represents the number of teeth of the gear connected to the motor shaft,  $g_2$  represents the number of teeth of the gear meshing with  $g_1$ ,  $g_3$  represents the number of teeth of the gear coaxial with  $g_2$ , and  $g_4$  represents the number of teeth of the sector gear.  $i_1$  represents the ratio of teeth between  $g_1$  and  $g_2$ , while  $i_2$  denotes the gear ratio between  $g_3$  and  $g_4$ .  $\theta_s$  represents the shift shaft angle of the shift actuator, a further term  $i_s$  represents the total speed ratio of the two-stage reduction mechanism,  $\omega_s$  represents the shift shaft speed of the shift actuator,  $x_{slv}$  represents the displacement of the engagement sleeve,  $L$  represents the length of the shift finger,  $T_s$  represents the torque of the shift shaft, and  $f_{slv}$  represents the thrust force on the sleeve.

### 2.3. System State Space

The displacement of the sleeve in this control system poses a measurement challenge; however, the known distance between the sleeve's movement from neutral to engagement with the target gear provides valuable information. An angle sensor is installed on the intermediate shaft of the shifting actuator, enabling us to determine the rotation angle of said shaft using Formula (4). The actuator intermediate shaft angle  $\theta_s$ , angular velocity  $\dot{\theta}_s$ , and angular acceleration  $\ddot{\theta}_s$  are the state variables;  $u$  is the control variable; and the intermediate shaft angle  $\theta_s$  is the output variable. Let  $x_1 = \theta_s$ ,  $x_2 = \dot{\theta}_s$ ,  $x_3 = \ddot{\theta}_s$ .

$$\left\{ \begin{array}{l} \dot{x}_1 = \dot{\theta}_s \\ \dot{x}_2 = \ddot{\theta}_s \\ \dot{x}_3 = \ddot{\theta}_s \\ y = x_1 \end{array} \right. \quad (5)$$

The simultaneous Equations (3)–(5) can be derived:

$$i_a = \frac{J_m \ddot{\theta}_m + b_m \dot{\theta}_m + T_L}{k_T} \quad (6)$$

$$\frac{di_a}{dt} = \frac{V_{bat} - R_a i_a - k_e \dot{\theta}_m}{L_a} \quad (7)$$

The substitution of Formula (6) into (7) yields the subsequent expression:

$$\frac{di_a}{dt} = \frac{K_T V_{bat} - R_a J_m \ddot{\theta}_m - R_a b_m \dot{\theta}_m - R_a T_L - K_T K_e \dot{\theta}_m}{L_a K_T} \quad (8)$$



The joint Formula (4) for the acceleration of sleeve displacement is expressed by the following equation, in accordance with Newton’s second law.

$$\frac{T_s}{L} = \frac{K_T i_a i_s}{L} = ma + F_L \tag{9}$$

The acceleration of the sleeve is represented by  $a$ , while the uncertain interference amount is denoted as  $F_L$ . The derivation of Formula (9) yields the following expression:

$$\frac{da}{dt} = \frac{K_T i_s}{mL} \frac{di}{dt} - \frac{\dot{F}_L}{m} \tag{10}$$

The derivation of Formula (11) is achieved by substituting Formula (6) with Formulas (7) and (8) into Formula (10).

$$\frac{da}{dt} = -\frac{K_T i_s}{mL} \left( \frac{K_T V_{bat} - R_a J_m \ddot{\theta}_m - R_a b_m \dot{\theta}_m - R_a T_L - K_T K_e \dot{\theta}_m}{L_a K_T} \right) - \frac{\dot{F}_L}{m} \tag{11}$$

Formula (4) is substituted into Formula (11) to obtain  $\ddot{\theta}_s$ :

$$\ddot{\theta}_s = -\frac{i_s^2 (R_a b_m + K_T K_e)}{mL^2 L_a} \dot{\theta}_s - \frac{R_a J_m i_s^2}{mL^2 L_a} \ddot{\theta}_s + \frac{k_T i_s}{mL^2 L_a} V_{bat} - \left( \frac{R_a T_L i_s}{mL^2 L_a} + \frac{\dot{F}_L}{mL} \right) \tag{12}$$

From the above equation, the system state equation can be derived as shown in the following equation:

$$\begin{cases} \dot{x}_1 = x_2 \\ \dot{x}_2 = x_3 \\ \dot{x}_3 = ax_2 + bx_3 + cu + d \\ y = x_1 \end{cases} \tag{13}$$

where  $a = -\frac{i_s^2 (R_a b_m + K_T K_e)}{mL^2 L_a}$ ,  $b = -\frac{R_a J_m i_s^2}{mL^2 L_a}$ ,  $c = \frac{k_T i_s}{mL^2 L_a}$ ,  $d$  is the disturbance of the system, and  $d = -\left(\frac{R_a T_L i_s}{mL^2 L_a} + \frac{\dot{F}_L}{mL}\right)$ . Then the system state equation can be finally written as Equation (14).

$$\begin{cases} \dot{x} = Ax + Bu + Ed \\ y = Cx \end{cases} \tag{14}$$

where  $A = \begin{pmatrix} 0 & 1 & 0 & 0 \\ 0 & 0 & 1 & 0 \\ 0 & a & b & -1 \\ 0 & 0 & 0 & 0 \end{pmatrix}$ ,  $B = \begin{pmatrix} 0 \\ 0 \\ c \\ 0 \end{pmatrix}$ ,  $E = \begin{pmatrix} 0 \\ 0 \\ 0 \\ 1 \end{pmatrix}$ , and  $C = (1 \ 0 \ 0 \ 0)$ .

### 3. Controller Design

#### 3.1. Trajectory Planning of Sleeve

Due to the absence of a unified dynamic model in the conventional AMT, it is commonly analyzed in multiple stages [13,16]. Naunheimer et al. [25] categorized this process into five stages and provided comprehensive explanations for each stage. The complete shifting process of the NSAMT system with a canceling synchronizer is accomplished through active angle alignment control and trajectory-tracking control of the shifting actuator, which can be further subdivided into three stages. In the initial stage, the Transmission Control Unit (TCU) initiates a shift instruction at the onset of gear shifting, triggering the activation of the shifting motor to position the sleeve in neutral. Subsequently, during the second stage, an active angle alignment control algorithm regulates the speed of the drive motor and governs the trajectory of both the sleeve and target gear throughout to minimize any gap between them. Once engagement occurs without collision between teeth on both components, completing a successful gear shift, we enter into a final third stage where

driving torque is restored. The process of active angle alignment during shifting is visually depicted in Figures 6 and 7.

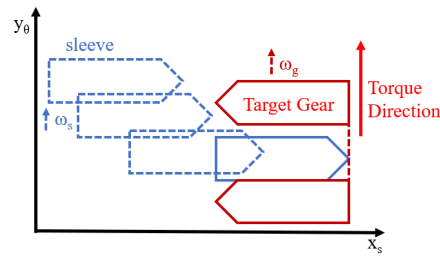


Figure 6. Shifting process of “active angle alignment”.

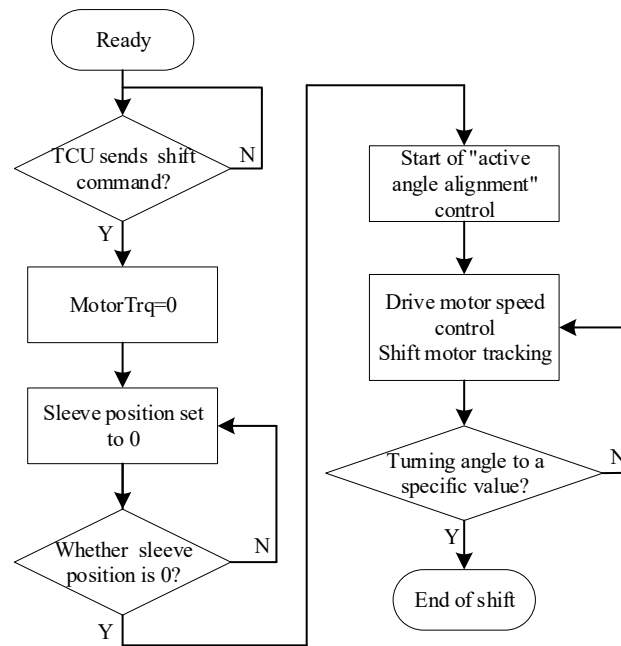


Figure 7. Active angle alignment control logic.

The essence of this process lies in the synchronous rotation and power transmission between two rotating bodies with rotational inertia and speed, achieved through the meshing of inner and outer teeth. Specifically, it involves the transverse cutting and meshing between the inner teeth of the engaging sleeve and the outer teeth of the target gear’s engaging gear ring. By considering both the engaging sleeve and target gear ring as separate rotating bodies, full engagement is achieved when their rotating centers align and their angular speeds match. If  $N$  represents the number of teeth on both the engaging sleeve and target gear ring, joint completion can be expressed using angles.

$$\begin{cases} \theta_{slv} = \theta_{gr} + k\frac{2\pi}{N}, k = 0, 1, 2 \dots N \\ \theta_{gr} = \theta_{slv} + k\frac{2\pi}{N}, k = 0, 1, 2 \dots N \end{cases} \quad (15)$$

The angle of the tooth ring to be engaged is represented by  $\theta_{gr}$ . Hence, the relationship between  $\theta_{slv}$  and  $\theta_{gr}$  throughout the entire process can be expressed as follows:

$$\theta_{slv}(t) = \theta_{gr}(t) + k\frac{2\pi}{N} + \Delta\theta(t), k = 0, \pm 1, \pm 2 \dots \quad (16)$$

where  $-\frac{\pi}{N} \leq \Delta\theta(t) < \frac{\pi}{N}$ ; at  $\Delta\theta(t) = 0$ , it can be assumed that the meshing docking angle of the two rotating bodies is fully aligned.

$$\Delta\theta(t) = \theta_{gr}(t) - \theta_{slv}(t) - k \frac{2\pi}{N}, k = 0, \pm 1, \pm 2 \dots \quad (17)$$

The angle difference between the internal and external gears, denoted as  $\Delta\theta(t)$  in Equation (17), can be calculated as  $2\pi/N$  minus half of the tooth spacing.

$$\Delta\theta(t) = \text{mod}_{\frac{2\pi}{N}}[\theta_{gr}(t) - \theta_{slv}(t)] - \frac{\pi}{N} \quad (18)$$

The incorporation of  $\theta_{slv}(t) = \int_0^t \omega_{slv} dt + \theta_{slv_0}$  and  $\theta_{gr}(t) = \int_0^t \omega_{gr} dt + \theta_{gr_0}$  into Equation (18) yields

$$\begin{aligned} \Delta\theta(t) &= \text{mod}_{\frac{2\pi}{N}} \left[ \int_0^t \omega_{slv} dt + \theta_{slv_0} - \int_0^t \omega_{gr} dt - \theta_{gr_0} \right] - \frac{\pi}{N} \\ &= \text{mod}_{\frac{2\pi}{N}} \left( \int_0^t \Delta\omega dt + \Delta\theta_{g0} \right) - \frac{\pi}{N} \end{aligned} \quad (19)$$

The variables  $\theta_{slv_0}$  and  $\theta_{gr_0}$  respectively denote the initial angle of the sleeve and the initial angle of the target gear ring. The equation  $\Delta\theta_{g0} = \theta_{slv_0} - \theta_{gr_0}$  holds, with radian as the unit.

The general relationship between the angular difference of two rotating bodies in relative motion can be expressed as the sum of  $\Delta\theta$  and  $k$  tooth spacing, where  $\Delta\theta(t) + k(t) \frac{2\pi}{N}$ . Both  $\Delta\theta$  and  $k$  are subject to change over time. However, for a specific tooth, the angular difference between the position where the target butt gear can mesh and align is always less than half of the tooth width, i.e.,  $|\Delta\theta(t)| \leq \frac{\pi}{N}$ .

The active angle alignment of dual-target tracking is conducted with the objectives of achieving "zero speed difference" and "zero angle difference". In this process, the relative speed and relative angle between the sleeve and the joint gear ring are considered as state variables in circumferential rotation, while the axial movement is characterized by the moving speed of the sleeve. The equation of state can be expressed as follows:

$$\begin{cases} \Delta\dot{\omega}_{slv-gr} = \frac{-i_{g0}i_{g1}}{J_{in}} \cdot T_m + \Delta f \\ \Delta\dot{\theta}_{slv-gr} = \Delta\omega_{slv-gr} \end{cases} \quad (20)$$

The initial state set in Formula (19) for active angle alignment control in dual-target tracking is defined as  $\Delta\omega_{g0} = \omega_{slv_0} - \omega_{gr_0}$  and  $\Delta\theta_{g0} = \theta_{slv_0} - \theta_{gr_0}$ . The termination conditions of the system are specified as  $\Delta\omega_{slv-gr}(t_f) = 0$  and  $\Delta\theta_{slv-gr}(t_f) = k \cdot (2\pi/N)$ , with a termination time of  $k = 0, 1, 2, \dots, t_f$ . The bi-objective control is further optimized to minimize the duration of the tracking control process. The performance functional of this procedure is set to

$$J = \int_{t_0}^{t_f} 1 dt \quad (21)$$

The optimization objectives are

$$T_m^* = \underset{T_m \in [-T_{\max}, T_{\max}]}{\text{argmin}} J \quad (22)$$

During the speed synchronization process, the motor generates maximum torque to minimize the speed deviation between the sleeve and gear ring. The torque output is adjusted based on both angular and velocity deviations. The vector control technique is employed for driving motors, while the PID control mechanism regulates any discrepancies in angle or speed differences. If  $|\Delta\theta(t)| > \frac{\pi}{N}$ , positive and negative output torques are determined by rotation direction until  $\Delta\omega_{slv-gr}$  and  $\Delta\theta_{slv-gr}$  reach their respective target values.

In the active angle alignment process, once the rotational speed and angle target of circumferential rotation are determined, it becomes essential to establish the axial motion trajectory of the sleeve. Ideally, when the base tooth tip of the sleeve moves from point A to point B,  $\Delta\omega$  should decrease to 0 while  $\Delta\theta$  changes to  $\theta_{adj}$ . This process is illustrated in Figure 8. By utilizing Equations (4) and (20), we can derive variations in  $\delta x_{slv}$ ,  $\delta\omega_{AB}$ , and  $\delta\theta_{AB}$  for points  $x_{slv}$ ,  $\Delta\omega$ , and  $\Delta\theta$  within a time sampling period  $T_s$ . Consequently, we can calculate the duration  $t_{AB}$  required for transitioning from point A to point B.

$$t_{AB} = \frac{x_{slv\_B} - x_{slv\_A}}{\delta x_{slv}} = \frac{H_l}{\delta x_{slv}} \tag{23}$$

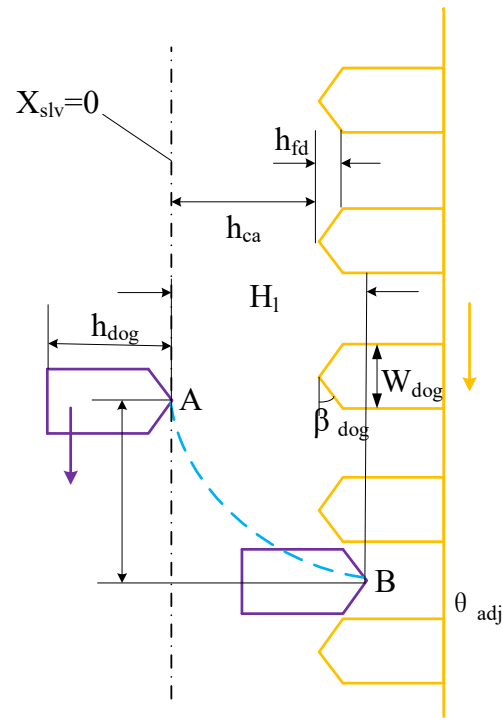


**Figure 8.** Gear engagement process from point A to point B. Two different colored arrows indicate the direction of motion.

In the equation  $H_l = h_{ca} + 2h_{fd}$ ,  $h_{ca}$  represents the distance between the teeth of the engaging gear ring when the engaging sleeve is in a neutral position.  $h_{fd} = \frac{W_{dog}}{2 \tan \beta_{dog}}$ , which signifies the axial distance between the tooth tip of the engaging gear ring and its maximum tooth width. Here,  $W_{dog}$  refers to the maximum tooth width of the engaging gear ring, while  $\beta_{dog}$  signifies the chamfer of its front tooth end face.

The axial velocity and displacement of the sleeve from points A to B can be determined by applying Formulas (4) and (23). Subsequently, the rotation angle of the intermediate shaft can be obtained based on the geometric relationship of the shifting actuator.

### 3.2. Design of Extended State Observer

The paper begins by constructing an extended state observer (ESO) to estimate the unknown state variables  $\theta_1$  and  $\theta_2$ . Subsequently, the controller utilizes the observation signal provided by ESO to design a control input  $u$  using a specific control algorithm. Finally, this control input is applied to the system under control, forming a closed-loop

feedback loop. The extended state observer is constructed for the purpose of system state observation. The design of the state observer is as follows:

$$\begin{cases} \dot{Z} = AZ + Bu + L_{ob}(y - \hat{y}) \\ \hat{y} = CZ \end{cases} \quad (24)$$

where  $Z = (x_1 \ x_2 \ x_3 \ x_4)^T$ ;  $L_{ob}$  denotes the observation matrix.

The observation matrix is set up using the pole configuration approach.

$$L_{ob} = (L_1 \ L_2 \ L_3 \ L_4)^T \quad (25)$$

The matrix of Equation (18) is full rank, and the system is observable according to the principle of observability.

$$\text{rank} = \begin{pmatrix} C \\ CA \\ CA^2 \\ CA^3 \end{pmatrix} = \begin{pmatrix} 1 & 0 & 0 & 0 \\ 0 & 1 & 0 & 0 \\ 0 & 0 & 1 & 0 \\ 0 & a & b & 1 \end{pmatrix} \equiv 4 \quad (26)$$

### 3.3. Trajectory Tracker Design

The shift motor is connected to the shift fork through a reduction gear, thereby amplifying the output torque and directly driving the shift fork. Consequently, any abnormal output torque is transmitted directly to the sleeve, potentially resulting in unpredictable phenomena. Similarly, any vibration and shock generated within the transmission system will also be transmitted to the sleeve. Furthermore, due to component wear and aging, certain parameters of the shift execution structure may undergo changes that introduce uncertainties affecting shift performance; hence, careful consideration must be given to ensure controller robustness. Based on the aforementioned analysis, the feedback controller is derived through the recursive construction of the Lyapunov function for the closed-loop system. The control law is carefully selected to ensure specific performance criteria for the derivative of the Lyapunov function along the trajectory of the closed-loop system, thereby guaranteeing boundedness and convergence of said trajectory towards its equilibrium point. The chosen control law represents a solution to various problems including system stabilization, tracking, interference suppression, or their synthesis [26]. To track and regulate planned trajectories, we employed the Backstepping method and conducted a simulation analysis. The complete design architecture is illustrated in Figure 9.

The control objective of the system is to precisely track the trajectory of the changing sleeve. As previously stated, the sleeve is tightly connected to the transmission system, and its linear trajectory can be converted into the rotation angle of the intermediate shaft through Formula (4). Therefore, our focus shifts towards tracking the rotation angle of said intermediate shaft. Let  $\hat{\theta}_s$  represent our desired target angle for said intermediate axis, and let  $e$  denote any error between this target angle and its actual value. This error can be expressed as Formula (27), which we will utilize in designing a control algorithm based on track-tracking principles aimed at eliminating errors.

The Backstepping method essentially employs Lyapunov's second method to facilitate state feedback design for the system controller, iteratively designing each state equation of the system in order to establish a control scheme [27]. Formulas (5) and (13) demonstrate that the system is a third-order system. Following the principle of Backstepping controller design, this process needs to be divided into three steps.

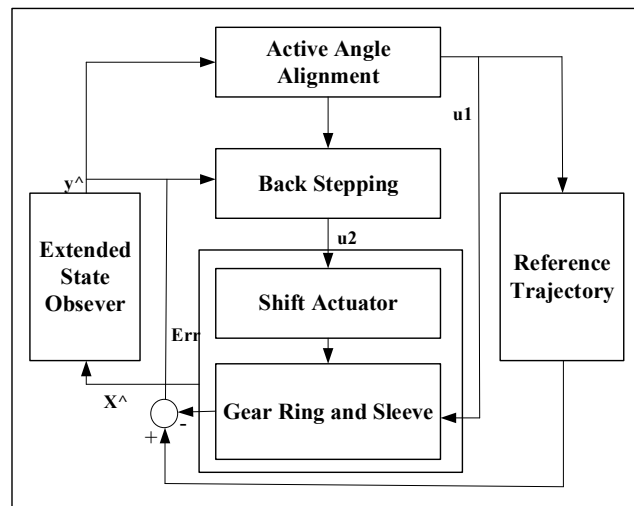


Figure 9. Controller design architecture.

$$e = \theta_d - \theta_s = x_{1d} - x_1 \tag{27}$$

First, the derivation of Equation (27) is obtained:

$$\dot{e} = \dot{x}_{1d} - \dot{x}_1 = \dot{x}_{1d} - x_2 \tag{28}$$

Step 1: Construct the Lyapunov function  $V(e)$  such that  $V(e)$  is positive definite and  $\dot{V}(e)$  is negative definite.

$$V_1 = \frac{1}{2}e^2 \tag{29}$$

The derivation of Equation (29) is as follows:

$$\dot{V}_1 = e\dot{e} = e(\dot{x}_{1d} - x_2) \tag{30}$$

If Equation (30) is made negative definite by making  $\dot{x}_{1d} - x_2 = -\lambda_1 e$ , where  $\lambda_1 > 0$ , then  $\dot{V}$  must be less than 0. So, for Equation (30) to be negative definite, it is necessary to make  $x_2 \rightarrow x_{2d}$ , and then the following equation can be obtained:

$$x_{2d} = \dot{x}_{1d} + \lambda_1 e \tag{31}$$

Step 2: Introduce the error  $\delta$ ,

$$\begin{cases} \delta = x_{2d} - x_2 \\ \dot{\delta} = \dot{x}_{2d} - \dot{x}_2 \end{cases} \tag{32}$$

Bringing Equation (32) into Equation (30) gives

$$\dot{V}_1 = e(\dot{x}_{1d} - (x_{2d} - \delta)) \tag{33}$$

Substituting Equation (31) into Equation (33) yields

$$\dot{V}_1 = -\lambda_1 e^2 + e\delta \tag{34}$$

$V_{2(e,\delta)}$  is constructed such that  $V_{2(e,\delta)}$  is positive definite and  $\dot{V}_{2(e,\delta)}$  is negative definite.

$$V_{2(e,\delta)} = V_1 + \frac{1}{2}\delta^2 \tag{35}$$

Derivation of Equation (35) gives

$$\dot{V}_2 = -\lambda_1 e^2 + \delta(e + \dot{\delta}) \quad (36)$$

Equation (32) is substituted into Equation (36).

$$\dot{V}_2 = -\lambda_1 e^2 + \delta(e + \dot{x}_{2d} - x_3) \quad (37)$$

If we want to make  $\dot{V}_2$  negative definite, then we can make  $e + \dot{x}_{2d} - x_3 = -\lambda_2 \delta$ , and then we can obtain

$$\begin{cases} x_3 = e + \dot{x}_{2d} + \lambda_2 \delta \\ x_3 \rightarrow x_{3d} \\ x_{3d} = e + \dot{x}_{2d} + \lambda_2 \delta \end{cases} \quad (38)$$

In the third step, the error  $\eta$  is introduced:

$$\begin{cases} \eta = x_{3d} - x_3 \\ \dot{\eta} = \dot{x}_{3d} - \dot{x}_3 \end{cases} \quad (39)$$

Equation (37) fused with Equations (38) and (39) can be rewritten as the following equation:

$$\dot{V}_2 = -\lambda_1 e^2 - \lambda_2 \delta^2 + \delta \eta \quad (40)$$

$V_{3(e,\delta,\eta)}$  is constructed as follows:

$$V_3 = V_2 + \frac{1}{2} \eta^2 \quad (41)$$

Derivation of Equation (41) yields

$$\dot{V}_3 = \dot{V}_2 + \eta \dot{\eta} = -\lambda_1 e^2 - \lambda_2 \delta^2 + \eta(\delta + \dot{\eta}) \quad (42)$$

$V_3$  is known to be positive definite, and if  $\dot{V}_3$  is to be negative definite, one can make  $\delta + \dot{\eta} = -\lambda_3 \eta$ , and then

$$\delta + (\dot{x}_{3d} - \dot{x}_3) = -\lambda_3(x_{3d} - x_3) \quad (43)$$

In Equation (43),  $\dot{x}_3$  is a function related to the control quantity  $u$ . Organizing each relation can lead to the control rate  $u$ , which satisfies Liapunov's second method with  $V_1, V_2, V_3$  positively determined and  $\dot{V}_1, \dot{V}_2, \dot{V}_3$  negatively determined.

$$u = [\ddot{x}_{1d} + (\lambda_2 + \lambda_3)\ddot{x}_{1d} + (\lambda_2\lambda_3 + 1)\dot{x}_{1d} + \lambda_1\dot{e} + (\lambda_1\lambda_3 + \lambda_1\lambda_2 + 1)\dot{e} + (\lambda_1\lambda_2\lambda_3 + \lambda_3 + \lambda_1)e - (\lambda_2\lambda_3 + a + 1)x_2 - (\lambda_3 + b)x_3 - d]/c \quad (44)$$

#### 4. Simulation and Analysis

The control algorithm developed above utilizes Matlab/Amesim for conducting joint offline simulation, wherein Amesim constructs the model of the controlled object and Matlab builds the model for the control algorithm, as depicted in Figure 10.

The shifting process from the first gear to the second gear was established, and the trajectory planning of the engaging sleeve was simulated and analyzed. The simulation results are presented in Figure 11.

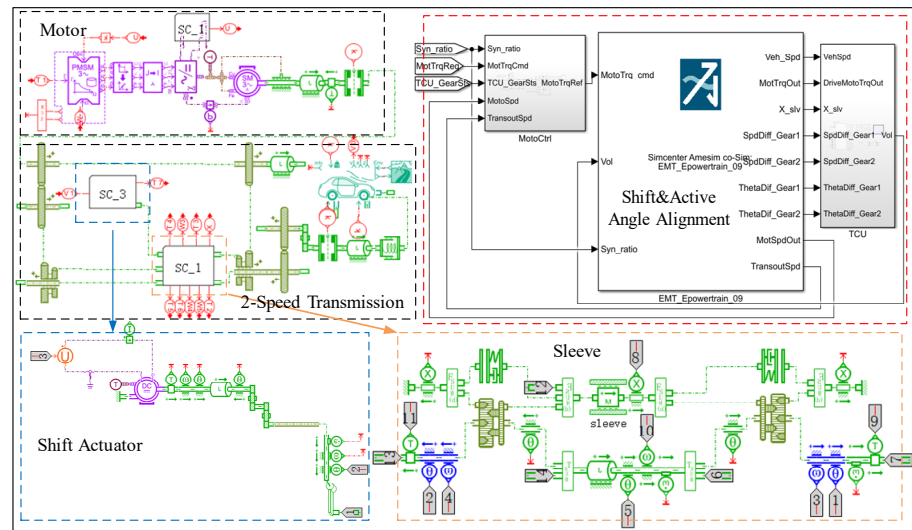


Figure 10. Matlab/AMESim co-simulation model.

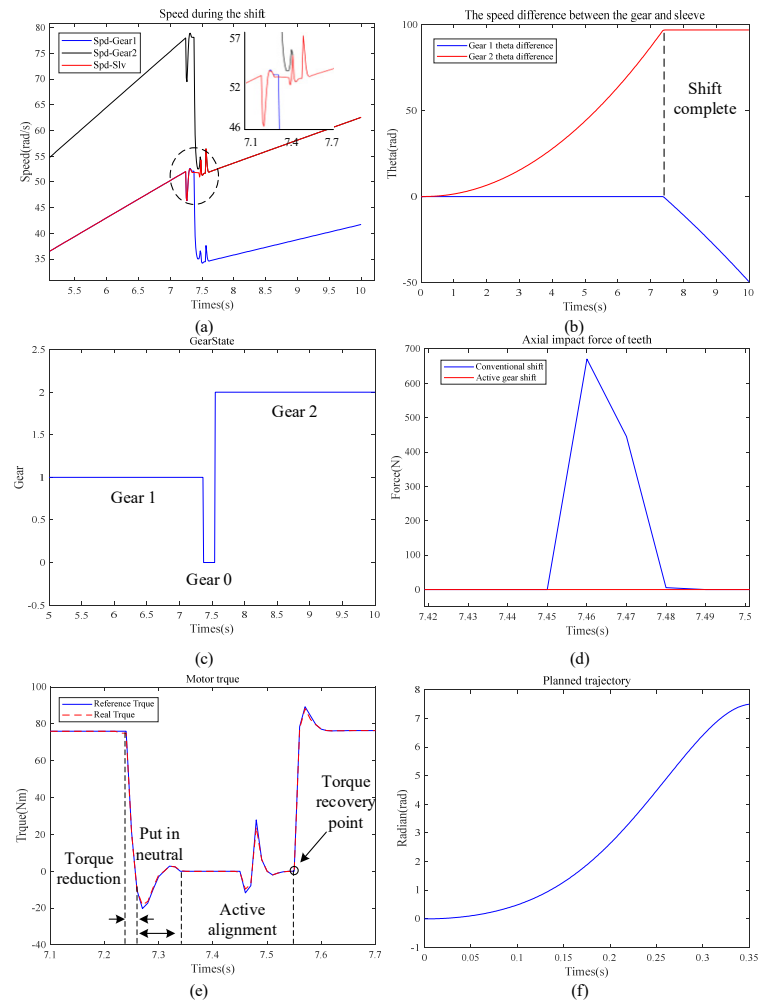


Figure 11. Trajectory-planning simulation of sleeve. (a) Gear speed during shift; (b) The speed difference between the gear and sleeve; (c) Gear state; (d) Axial impact force of teeth; (e) Motor torque; (f) Planned trajectory.

Figure 11 depicts a simulation diagram of engagement gear trajectory planning utilizing active angle alignment. As shown in Figure 11a, throughout the entire simulation



process, the gear ring speed of gear 1 remains consistent with that of the engagement sleeve. Upon reaching the gear-shifting point, the engagement sleeve is disengaged from gear 1's ring by means of the gear-shifting actuator and enters into a free movement stage before being actively controlled to engage with gear 2. This process demonstrates that the active angle alignment algorithm can be effectively applied to this system. The rotation angles of the gear rings at different gear positions and their differences with the rotation angles of the sleeve are illustrated in Figure 11b. Following the completion of the gear shift, a certain disparity is maintained between the rotation angles of the second gear ring and those of the sleeve, aligning with Formula (19). The shift change diagram of the entire shift process is depicted in Figure 11c, illustrating a total duration of approximately 350 ms. Figure 11d demonstrates the axial collision between the traditional gear and the active angle alignment, wherein the utilization of the active angle alignment algorithm for shift control effectively mitigates meshing gear collisions. The optimized drive motor torque and actual motor torque during the entire shift process are presented in Figure 11e. It can be observed from this figure that there is a strong correspondence between the actual torque and desired values, thereby validating the efficacy of drive motor control. Lastly, Figure 11f showcases the planned axial movement path of the sleeve, which is derived by converting Formula (4) into an intermediate shaft rotation angle.

The parameters of the NSAMT shift actuator are shown in Table 1.

**Table 1.** The parameters of the NSAMT shift actuator.

Controller Parameters		
Parameter	Parameter Symbol	Parameter Value
Power supply voltage	$V_{bat}$	12 V
The torque coefficient	$K_T$	0.02 Nm/A
Back emf coefficient	$K_e$	0.12 v·s/rad
Electrical resistance	$R_a$	0.47 ohm
The motor inductance	$L_a$	0.0216 H
The moment of inertia	$J_m$	0.0008 kg/m <sup>2</sup>
Total speed ratio of reduction mechanism	$i_s$	20
The length of the shift fork	$L$	0.02 m
Motor damping coefficient	$b_m$	0.005 Nm/rad

The Backstepping algorithm is configured with  $\lambda_1 = 80$ ,  $\lambda_2 = 90$ ,  $\lambda_3 = 12$ . In accordance with the shift process, a time-varying interference amount is introduced, and the control input range is set to  $[-12 \ 12]$ . As a point of comparison, the PID algorithm is selected, and the simulation results are presented below.

The simulation results of trajectory tracking under the Backstepping algorithm, presented in Figure 12, are highly satisfactory compared to those obtained using PID control. Figure 12a includes an enlarged diagram of the simulation results at both ends and demonstrates a minimal deviation at joints for both algorithms. Figure 12b presents the control input for each algorithm, while Figure 12c displays the tracking error. Finally, Figure 12d illustrates a substantial variation during the initial and final stages in convergence speed between the two algorithms.

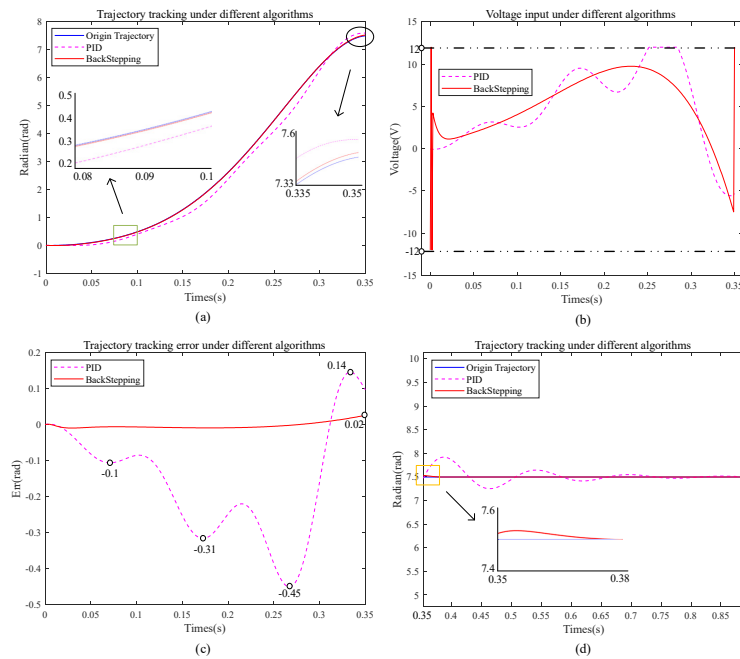


**Figure 12.** Trajectory tracking effects under different algorithms. (a) Trajectory tracking under different algorithms; (b) Voltage input under different algorithms; (c) Trajectory tracking error under different algorithms; (d) convergence speed between the two algorithms.

### 5. Experiment and Conclusions

#### 5.1. HIL Test

The proposed strategy in this paper was further validated for its real-time capability and effectiveness through HIL testing conducted on the Dspace platform (ControlDesk 7.0). The HIL test setup is illustrated in Figure 13.

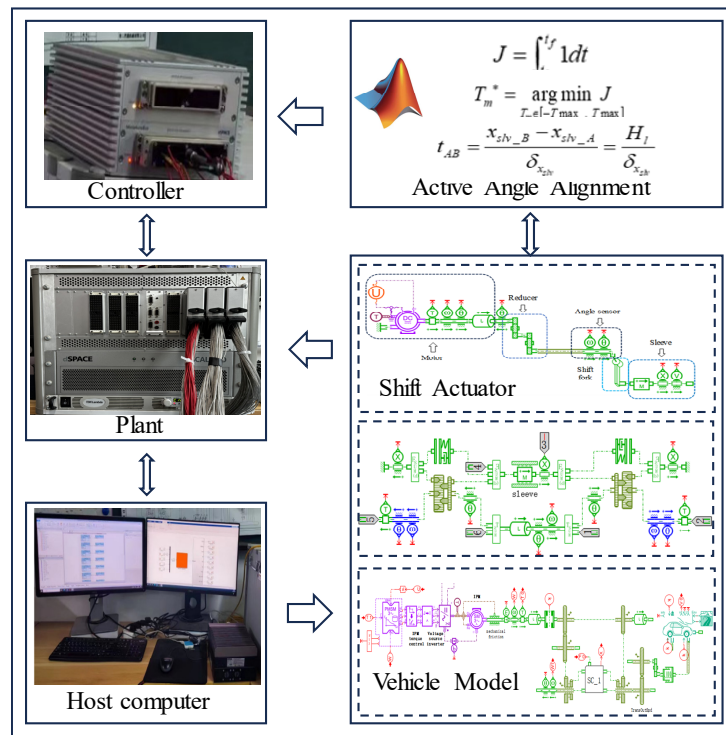


**Figure 13.** HiL test platform.

The controlled object model was imported to the lower computer via Ethernet, and the control algorithm simulation environment was configured with a fixed time step of 1000 Hz. The code was then compiled and downloaded to the controller. The simulation results are depicted in Figure 14.

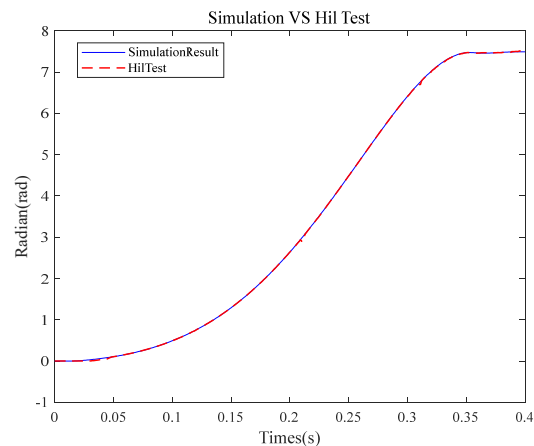


**Figure 14.** Comparison between HiL test and simulation of Backstepping algorithm.

The comparison diagram in Figure 14 illustrates the HiL test and simulation results of the Backstepping algorithm. It is evident from the diagram that although there is a slight lag in response time and minor errors at the end of the HiL test, overall, both approaches exhibit substantial similarity. Thus, it can be inferred that the real-time capability and effectiveness of the control strategy are validated through HiL testing.

## 5.2. Conclusions

- (1) The designed active angle alignment algorithm effectively plans the motion trajectory of the sleeve, ensuring collision-free engagement between the sleeve and the target gear ring.
- (2) The HiL test results align closely with the simulation results, validating the accurate control of the NSAMT gear-shifting actuator through the proposed Backstepping algorithm. This provides a valuable reference for controlling transmission gear-shifting actuators with similar structures.
- (3) The control strategy constructed in this article can ensure fast gear shifting while avoiding circumferential collisions and impacts between the gear ring and the joint sleeve, reducing wear on the parts.

**Author Contributions:** Methodology, X.G. and C.D.; Software, L.L., J.W. and Z.D.; Formal analysis, C.H. All authors have read and agreed to the published version of the manuscript.

**Funding:** This research was funded by Key R&D project of Guangxi Province, China grant number AA23062058 and Key R&D project of Hubei Province, China grant number 2022BAA074.

**Data Availability Statement:** The data are not publicly available due to restrictions of company, their containing information that could compromise the privacy of research participants.

**Conflicts of Interest:** Author Zhengli Dai was employed by the company Chongqing Tiema Industries Group Co., Ltd. The remaining authors declare that the research was conducted in the absence of any commercial or financial relationships that could be construed as a potential conflict of interest.

## References

1. Tseng, C.Y.; Yu, C.H. Advanced shifting control of synchronizer mechanisms for clutchless automatic manual transmission in an electric vehicle. *Mech. Mach. Theory* **2015**, *84*, 37–56. [[CrossRef](#)]

2. Lei, Y.; Zhang, Y.; Fu, Y.; Yan, B. Accurate Control of AMT Gear Shifting Based on Fuzzy Adaptation. In Proceedings of the 2017 2nd International Conference on Materials Science, Machinery and Energy Engineering (MSMEE 2017), Dalian, China, 13–14 May 2017. [[CrossRef](#)]
3. Hu, J.; Ran, H.; Pang, T.; Zhang, Y. Parameter design and performance analysis of shift actuator for a two-speed automatic mechanical transmission for pure electric vehicles. *Adv. Mech. Eng.* **2016**, *8*, 1–15. [[CrossRef](#)]
4. Zhu, X.; Zhang, H.; Xi, J.; Wang, J.; Fang, Z. Robust speed synchronization control for clutchless automated manual transmission systems in electric vehicles. *Proc. Inst. Mech. Eng. Part D J. Automob. Eng.* **2014**, *229*, 424–436. [[CrossRef](#)]
5. Li, W.; Kang, C.; Zhu, X. Coordinated speed and position control of integrated motor-transmission system. *Trans. Inst. Meas. Control.* **2021**, *43*, 3013–3023. [[CrossRef](#)]
6. Lu, Z.; Chen, H.; Wang, L.; Zeng, Y.; Ren, X.; Li, K.; Tian, G. Gear-shifting control of non-synchronizer electric-driven mechanical transmission with active angle alignment. *Optim. Control. Appl. Methods* **2022**, *43*, 322–338. [[CrossRef](#)]
7. Barrientos, E. *Model Based Control of Synchronizers for Reducing Impacts during Sleeve to Gear Engagement*; SAE International: Warrendale, PA, USA, 2019. [[CrossRef](#)]
8. Kumbhar, M.S.; Panchagade, D.; Baidya, K. Development of DC Motor Controlled Automated Manual Transmission (AMT). *Int J. Recent Technol. Eng.* **2014**, *3*, 124–129.
9. Wang, X.; Li, L.; He, K.; Liu, C. Dual-loop self-learning fuzzy control for AMT gear engagement: Design and experiment. *IEEE Trans. Fuzzy Syst.* **2017**, *26*, 1813–1822. [[CrossRef](#)]
10. Yan, F.; Wang, J.; Du, C.; Hua, M. Multi-Objective Energy Management Strategy for Hybrid Electric Vehicles Based on TD3 with Non-Parametric Reward Function. *Energies* **2023**, *16*, 74. [[CrossRef](#)]
11. Wang, S.; Fan, Z.X.; Li, B.L.; Gao, S.; Cui, G.; Li, P.; Wu, J.; Yin, C. Research on Control of AMT Shift Actuator Based on Backstepping. In Proceedings of the 2022 6th CAA International Conference on Vehicular Control and Intelligence (CVCI), Nanjing, China, 28–30 October 2022; pp. 1–5.
12. Lin, S.; Chang, S.; Li, B. Gearshift control system development for direct-drive automated manual transmission based on a novel electromagnetic actuator. *Mechatronics* **2014**, *24*, 1214–1222. [[CrossRef](#)]
13. Lin, S.; Li, B. Shift Force Optimization and Trajectory Tracking Control for a Novel Gearshift System Equipped with Electromagnetic Linear Actuators. *IEEE/ASME Trans. Mechatron.* **2019**, *24*, 1640–1650. [[CrossRef](#)]
14. Xu, X.; Luo, Y.; Hao, X. Coordinated shift control of nonsynchronizer transmission for electric vehicles based on dynamic tooth alignment. *Front. Mech. Eng.* **2021**, *16*, 887–900. [[CrossRef](#)]
15. Li, B.; Ge, W.; Yu, X.; Shao, S.; Liu, H. Innovative design and gearshift control for direct-drive electromagnetic gearshift system equipped with servo synchronizer. *Proc. Inst. Mech. Eng. Part D J. Automob. Eng.* **2018**, *233*, 1115–1124. [[CrossRef](#)]
16. Pan, T.; Zang, H.; Wu, P. Hierarchical mode optimization strategy for gear engagement process of automated manual transmission with electromagnetic actuator. *Proc. Inst. Mech. Eng. Part D J. Automob. Eng.* **2023**, *237*, 913–929. [[CrossRef](#)]
17. Chen, H.K.G. Optimal preview position control for shifting actuators of automated manual transmission. *Proc. Inst. Mech. Eng. Part D J. Automob. Eng.* **2019**, *233*, 440–452. [[CrossRef](#)]
18. Zhang, H.; Zhang, Y.; Hao, C.; Lu, Y. Test Research on Optimization of AMT Shift Control Parameters. In Proceedings of the 2021 5th CAA International Conference on Vehicular Control and Intelligence (CVCI), Tianjin, China, 29–31 October 2021; pp. 1–6.
19. Feng, T.; Lijun, W.; Liqi, S.; Yuanfan, Z.; Xingyue, Z.; Guangyu, T. Active synchronizing control of transmission shifting without a synchronizer for electric vehicles. *J. Tsinghua Univ. (Sci. Technol.)* **2020**, *60*, 101–108.
20. Yuanfan, Z.; Hongxu, C.; Lijun, W.; Guangyu, T.; Weibo, Z. Modeling and control of gear shifting of a non-synchronizer motor-transmission drive system. *J. Tsinghua Univ. (Sci. Technol.)* **2020**, *60*, 910–919.
21. Xu, X.; Luo, Y. Modeling and analysis of gear shifting process of non-synchronizer AMT based on collision model. *IEEE Access* **2021**, *9*, 13354–13367. [[CrossRef](#)]
22. Lu, Z.; Tian, G.; Onori, S. Multistage time-optimal control for synchronization process in electric-driven mechanical transmission with angle alignment considering torque response process. *J. Dyn. Syst. Meas. Control.* **2021**, *143*, 041006. [[CrossRef](#)]
23. Pravika, M.; Jacob, J.; Joseph, K.P. Design of linear electromechanical actuator for automatic ambulatory Duodopa pump. *Eng. Sci. Technol. Int. J.* **2021**, *31*, 101056. [[CrossRef](#)]
24. Li, L.; Wang, X.; Hu, X.; Chen, Z.; Song, J.; Muhammad, F. A Modified Predictive Functional Control with Sliding Mode Observer for Automated Dry Clutch Control of Vehicle. *J. Dyn. Syst. Meas. Control.* **2016**, *138*, 061005. [[CrossRef](#)]
25. Lechner, G.; Naunheimer, H. *Automotive Transmissions: Fundamentals, Selection, Design and Application*; Springer: Berlin, Germany, 2011.
26. Chen, C.; Yu, H. Backstepping sliding mode control of induction motor based on disturbance observer. *IET Electr. Power Appl.* **2020**, *14*, 2537–2546. [[CrossRef](#)]
27. Errami, Y.; Obbadi, A.; Sahnoun, S. Development of a Nonlinear Backstepping Approach of Grid-Connected Permanent Magnet Synchronous Generator Wind Farm Structure. In *Renewable Energy Systems*; Elsevier: Amsterdam, The Netherlands, 2021.

**Disclaimer/Publisher’s Note:** The statements, opinions and data contained in all publications are solely those of the individual author(s) and contributor(s) and not of MDPI and/or the editor(s). MDPI and/or the editor(s) disclaim responsibility for any injury to people or property resulting from any ideas, methods, instructions or products referred to in the content.